A NUMERICAL STUDY OF BUBBLES CAPTURED BY A GAUSSIAN VORTEX

Claudia Iyer
University of Michigan
Ann Arbor, MI 48109

Giuseppe Sassanelli
Politecnico of Bari
Bari, Italy 70124

Gretar Tryggvason
Worcester Polytechnic Institute
Worcester, MA 01609-2280

Steven Ceccio
University of Michigan
Ann Arbor, MI 48109

Abstract

The capture mechanics of cavitation nuclei by a Gaussian Vortex is explored. The capture process is examined by both Direct Numerical Simulation of the Navier Stokes equations and a Particle Tracking model. We also investigate the parameters that effect the capture and bubble growth process, and finally we compare the results of the two approaches. The DNS results show that the shape of the bubbles can be significantly distorted as they are captured by a vortex. This distortion can lead to the creation of lift forces that shorten the capture time of the bubbles. The capture times computed with the two methods varied over less than an order of magnitude for most cases, and this suggests that one might derive and average capture time. The exact results of the particle tracking models can vary widely depending on the selected values of the lift and drag coefficients and nominal Weber number of the captured nucleus. For model scale flows, the Weber number may vary from 1 to 100. Thus, it is possible that a particle-tracking model should have variable lift and drag coefficients that better take into account the estimated instantaneous bubble deformation. The drag coefficient by Haberman and Morton (1953) yielded a trajectory that was closer to the DNS trajectory than when using the drag coefficient given by Clift et al.(1978). It was determined that the lift coefficients given by Dandy and Dwyer (1990) and Auton et al. (1988) yielded capture times that were much bigger than the DNS results and that lift coefficient between the those given by Saffman (1965) and Dandy and Dwyer (1990) would give results that are closer to the DNS results.

1 Introduction

Device such as propellers and axial pumps can exhibit Tip Vortex Cavitation or Tip Leakage Vortex Cavitation. Tip vortices occur at the termination of lifting surfaces, and small bubbles (nuclei) can be captured by the strong vortex. If the pressure falls below vapor pressure within the vortex core, the bubbles may cavitate. The interaction and growth of small bubbles with a concentrated vortex has been examined by several researchers. For example, Sridhar and Katz (1999) studied the effect of an entrained bubble in a vortex-ring using particle imaging velocimetry. They showed that often the entrained bubble can substantially change the structure of the vortex. Chahine (1990), (1994) studied how bubbles are captured and deformed by a vortex. Hsiao et al. (1999) examined the capture of cavitation nucleus by a tip vortex using employing both a RANS flow field simulation and a particle tracking model. Models of vortex cavitation often use the spherical Rayleigh-Plesset equation to describe the dynamics of the cavitating bubbles. This approach assumes that the dynamic of the bubble keeps a spherical symmetry during the growth and the collapse. Therefore the bubble lift and the drag coefficients are determined using empirical equation for spherical body. However, the cavitation bubble can be deformed by the vortex as it grows, losing its spherical shape. This will

change the effective lift and drag coefficients of the bubble. Direct Numerical Simulation of the cavitating bubble can be used to examine this effect and to determine the extent to which deforming cavitation bubbles depart from particle tracking models. In the present work, the interaction between a vortex and a deforming cavitation bubble will be examined using a Direct Numerical Simulation (DNS) Front Tracking Model for multiphase flows. These bubbles have either a constant or variable gas pressure with changing bubble volume. Validations cases have been run with variations in spatial resolution and preliminary comparisons have been made with a simple particle tracking model. The simulations have shown significant difference in the trajectory, capture time and growth rate of the bubble between DNS an Particle Tracking. Different lift and drag coefficients have been used in order to determine which give closest trajectory and capture time to the DNS .

2 Numerical Method

The numerical method used in this study to compute the Navier-Stokes equations is a Direct Numerical Simulation (DNS) front- tracking method for multiphase flows developed by Unverdi and Tryggvason (1992) and improved by Esmaeeli and Tryggvason (1998, 1999). The fluids inside and outside the bubbles are taken to be Newtonian and the flow is incompressible and isothermal, so that the densities and viscosities are constant within each phase. The unsteady, viscous, incompressible Navier-Stokes equations are solved by a finite-difference approximation on a fixed staggered grid, while the interface between the bubbles and fluid were explicitly represented by a separate, unstructured grid that moves through the stationary one. The front (interface) keeps the density and viscosity discontinuities sharp and also provides means for calculation of the surface tension forces. A numerical method based on the Marker-And-Cell method developed by Harlow and Welch (1965) is used to solve the unsteady Navier-Stokes equations over the entire computational domain. This "one-field" formulation, which computes both the properties within the bubbles and in the ambient fluid, is used in conjunction with a linked list of markers that is used to explicitly track the position of the fluid interfaces. A single Navier-Stokes equation with variable density, ρ and viscosity, μ is solved for the entire domain. The momentum equation and the conservation of mass for an incompressible system can be written in conservative form as:

$$\frac{\partial \rho \boldsymbol{u}}{\partial t} = \boldsymbol{\nabla} \cdot \rho \boldsymbol{u}\boldsymbol{u} - \boldsymbol{\nabla} p + \rho \boldsymbol{g} + \boldsymbol{\nabla} \cdot \mu(\boldsymbol{\nabla}\boldsymbol{u} + \boldsymbol{\nabla}^{\boldsymbol{T}}\boldsymbol{u}) + \int_A \sigma k \boldsymbol{n} \delta(x - x_f) dA \tag{1}$$

$$\boldsymbol{\nabla} \cdot \boldsymbol{u} = 0 \tag{2}$$

where $\boldsymbol{u}$ denotes the velocity vector, $\boldsymbol{p}$ the pressure, $\boldsymbol{g}$ the gravity acceleration field, $\boldsymbol{\sigma}$ the surface tension, k is the curvature for two-dimensional flow and twice the mean curvature of the interface for three-dimensional flows, $\boldsymbol{n}$ is the unit vector normal to the front, dA is the area element on the front, $\delta(x - x_f)$ is a delta-function which is zero everywhere except at the interface where $x = x_f$, x is the point at which the equation is evaluated, and x_f is a point on the front. The last term of the momentum equation is the surface tension, which is added as a body force concentrated at the interface and the integration is over the bubble surface. Both fluids are assumed to be incompressible, so the Navier-Stokes equations are supplemented by the incompressibility condition, Equation 2. The front tracking code has been modified to accommodate cavitation. For the cavitation problem, the equations for the conservation of mass and momentum are solved on a regular, fixed grid in both two- and three-dimensional coordinates. Again, the numerical scheme used is a conservative second-order accurate, centered difference scheme for spatial variables, and explicit second-order time integration. The numerical treatment of cavitation is discussed here. Two cavitation models were used. The first one assumes that the pressure of the fluid within the bubble is constant and equal to the fluid vapor pressure:

$$P_{inside} = P_{vap} \tag{3}$$

In the numerical scheme, this is accomplished in the solution of the pressure field. The second cavitation model allows for variable pressure inside the bubble, the pressure depending on the volume of the bubble as follows:

$$P_{inside} = P_{vap} + P_{gas,i}\frac{V_0}{V} \tag{4}$$

where Pinside is the pressure inside the bubble, P_{vap} is the water vapor pressure, $P_{gas,i}$ is the initial partial pressure of the non-condensable gases, V_0 is the initial volume of the bubble, and V is the volume of the bubble. Here, it is assumed that the non-condensable gases follow an isothermal expansion. In the cavitation problems, additional pressure boundary conditions are assigned along one or more sides of the computational domain. For the collapse of a bubble in an unbounded fluid, constant pressure boundary conditions are assigned on all six sides of the 3-D domain. For the collapse of a bubble near a wall, constant pressure boundary conditions are assigned on the top of the domain. For growth and collapse of bubbles in concentrated vortices constant pressure boundary conditions are assigned along the outer edges of the vortex and periodic boundary conditions along the axis of the vortex.

3 Particle Tracking Model

It is often desired to estimate when cavitation inception might occur through the examination of the otherwise known cavitating flow field. For example, numerical simulations of the non-cavitating flow may be used to find the region of the lowest pressures. A further refinement is to place nuclei in the flow as Lagrangian traces and allow them to be convected into regions of low pressure. The dynamics of the particles can then be calculated assuming that their presence in the flow does not significantly alter the non-cavitating flow. These are often called "one-way coupled" particle tracking models. The effect of the flow on a bubble or particle can be determined through the equation of motion for the particle. By considering all forces acting on a spherical particle, the equation of motion (Maxey and Riley, 1983) of a particle of mass m_p and velocity up in a gravity field $\boldsymbol{g}$ is written as:

$$m_p\frac{d\boldsymbol{u}}{dt} = (m_p - m_f)\boldsymbol{g} + \ m_f\frac{D\boldsymbol{U_f}}{dt} + \boldsymbol{F_A} + \boldsymbol{F_D} + \boldsymbol{F_L} + \boldsymbol{F_H} \tag{5}$$

where m_F is the mass of the fluid enclosed in the volume of the particle, U_F is the fluid velocity in the absence of the particle at the center of the particle (the unperturbed velocity), is the total derivative and represents the Lagrangian fluid acceleration. The forces exterded by the outer flow on the particle are: the added-mass force $\boldsymbol{F_A}$, the drag force $\boldsymbol{F_D}$, the lift force $\boldsymbol{F_L}$, and the Basset history force $\boldsymbol{F_H}$. The above equation of motion is valid for spherical particles and bubbles with radii that are smaller than the largest scales of the flow. The equation of motion 5 describes the motion of a solid particle in the flow. To describe the equation of motion of a bubble one may need to take into account the force due to the bubble volume variation. By adding an additional term to consider the bubble volume variation and neglecting the Basset history term, Equation 5 can be written as:

$$m_p\frac{d\boldsymbol{u}}{dt} = (m_p - m_f)\boldsymbol{g} + \ m_f\frac{D\boldsymbol{U_f}}{dt} + \boldsymbol{F_A} + \boldsymbol{F_D} + \boldsymbol{F_L} + \boldsymbol{F_V} \tag{6}$$

where the additional term related to the bubble volume variation is given by Johnson and Hsieh (1966) as:

$$\boldsymbol{F_V} = 2\pi R^2\rho_F(\boldsymbol{U_f} - \boldsymbol{u_p})\frac{dR}{dt} \tag{7}$$

where R is the bubble radius. The added mass $\boldsymbol{F_A}$ is equal to one-half the mass of the displaced liquid volume:

$$\boldsymbol{F_A} = \frac{2}{3}\pi R^3\rho_F \tag{8}$$

To determine the volume variation for a spherical bubble, the Rayleigh-Plesset equation given by Plesset (1948) is used:

$$R\frac{d^2R}{dt^2} + \frac{3}{2}(\frac{dR}{dt})^2 = \frac{1}{\rho}(P_{vap} + P_{gas,i}\frac{V_0}{V} - p - \frac{2\sigma}{R} - \frac{4\mu}{R}\frac{dR}{dt}) \tag{9}$$

where P_{vap} is the liquid vapor pressure, $P_{gas,i}$ is the initial partial pressure of the non-condensable gases, p is the ambient pressure, V_0 is the initial volume of the bubble, V is the volume of the bubble, σ is the

surface tension, and μ is the dynamic viscosity. Here, an isothermal expansion of the bubble is assumed and the bubble is assumed to remain spherical.

4 Gaussian Vortex

For the computations of bubbles in a Gaussian vortex, the flow is initialized with a Gaussian vortex of radius r and strength Γ. The Gaussian vortex, also known as Lamb-Oseen vortex (Lamb, 1932, Saffman, 1992) is the simplest viscous vortex in which the initial vorticity is $\omega(r,0) = 0$ and the vorticity at a radius, r, and a later time, t, is given by:

$$\boldsymbol{\omega} = \frac{\Gamma_0}{4\pi\nu t} e^{\frac{-r^2}{4\nu t}} \tag{10}$$

The tangential velocity around the axis is given by:

$$\boldsymbol{u} = \frac{\Gamma_0}{2\pi r}(1 - e^{\frac{-r^2}{4\nu t}}) \tag{11}$$

where Γ is the vortex strength and ν is the viscosity. This corresponds to an isolated vortex of strength Γ_0 concentrated on the z-axis at time 0. As time increases from 0 to ∞, the velocity diminishes from $\Gamma_0/(2\pi r)$ to 0. The circulation around a circle of radius r is given by:

$$\Gamma = \int_0^r \omega \cdot 2\pi r dr = \Gamma_0(1 - e^{\frac{-r^2}{4\nu t}}) \tag{12}$$

The maximum tangential velocity, U_{core}, occurs at the core radius, r_{core}. The maximum velocity can be written as:

$$U_{core} = \frac{\Gamma_0}{2\pi r_{core}}(1 - e^{\frac{-r_{core}^2}{4\nu t}}) = (0.7147)\frac{\Gamma_0}{2\pi r_{core}} \tag{13}$$

The tangential velocity profiles of a tip vortex generated by a three-dimensional foil were measured by Boulon et al. (1999) using Laser Doppler Velocimetry for a Reynolds of 10^6 based on chord lenght. They found that the vortex core radius, R_{core}, was on the order of 2.5 mm and that the maximum core velocity, U_{core}, was on the order of 5 m/s. This yields a vortex strength of $\Gamma = 0.0785 m^2/s$. In the simulations presented here the core radius was chosen to be $r_{core} = 2.5$ mm and the maximum tangential velocity $U_{core} = 5$ m/s. The position and size were non-dimensionalized by the length of the computational domain, L = 10 mm, the velocities were non-dimensionalized by $2U_{core} = 10$ m/s, and the time was non-dimensionalized by $t = L/2U_{core}$ =0.001s. In this study, the Weber number was defined as:

$$We = \frac{\rho D_b U_{core}^2}{4\sigma} \tag{14}$$

The boundary conditions used in this study imposed a constant pressure on the boundary and allowed for inflow or outflow as the bubble changes its volume. A Reynolds number associated with the vortical flow is defined as:

$$Re = \frac{D_{core} U_{core}}{\nu} \tag{15}$$

where D_{core} is the diameter of the viscous core and ν is the kinematic viscosity. The cavitation number is defined as:

$$\sigma = \frac{P_\infty - P_{vap}}{\frac{1}{2}\rho U_{core}^2} \tag{16}$$

where P_∞ is the freestream pressure and ρ is the density. The freestream pressure is imposed on the boundary of the computational domain.

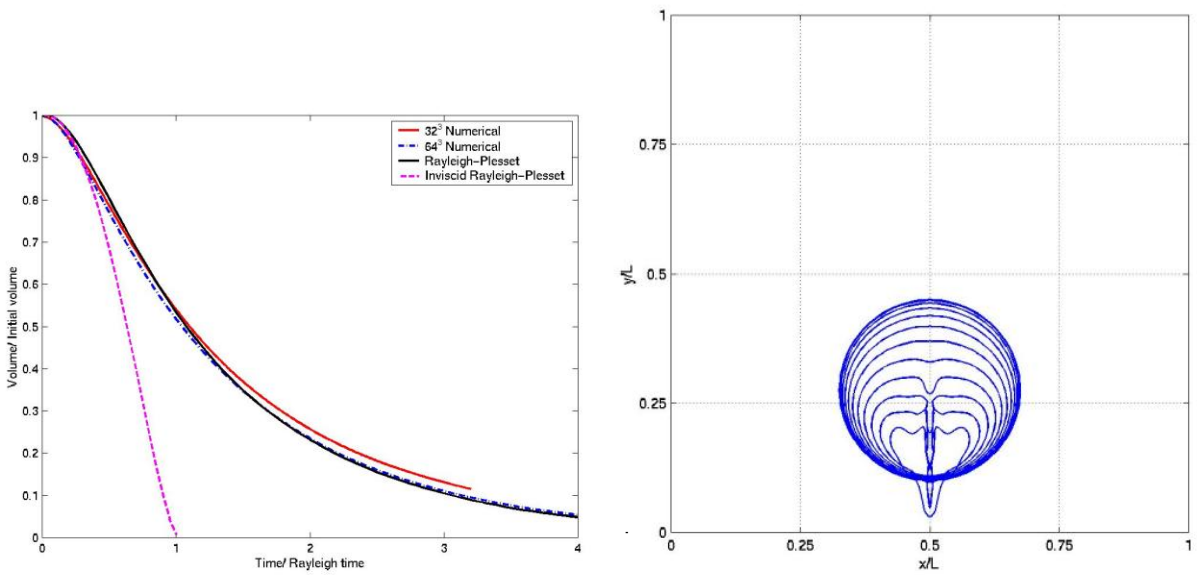

Figure 1: 1a Left: Collapse of a spherical bubble in an unbounded fluid. 1b Right: Collapse of a spherical bubble near a wall. The surface bubble from time $t/t_r = 0.0$ to $t/t_r = 1.25$ is shown.

5 Validation Tests

In order to assess the accuracy of the implementation of the cavitation model in the Direct Numerical Simulations (DNS) code, the collapse of a bubble in an unbounded fluid was computed and compared to the analytical solution given by Rayleigh (1917). DNS computations of bubble collapse in an unbounded viscous fluid were done in a three-dimensional domain with two different resolutions of 32^3 and 64^3 cells and the results were compared with the analytical solution given by the Rayleigh-Plesset equation. The cavitation model used assumed that the pressure inside the bubble was equal to the vapor pressure. Figure 1a shows the dimensionless bubble volume, which is V/V_0, plotted vs. the dimensionless time, which is t/t_R, for both grid resolutions as well as the theoretical result. The theoretical result for the collapse of a bubble in an inviscid fluid is also plotted in Figure 1a for comparison. As expected, the collapse of the bubble in a viscous fluid has a reduced bubble collapsing rate than that in an inviscid fluid. For the simulations shown, the length of the computational domain are twice the diameter of the initial bubble and the bubble was placed in the center of the domain. The Reynolds number based on the collapse velocity is $Re = 1$, the Rayleigh time is $t_R = 1.25$, and the surface tension was neglected. Another test for determining the accuracy of the implementation of the cavitation model in the DNS code was done by computing the collapse of a bubble near a wall. When bubbles collapse near a wall, a jet of liquid, called the "re-entrant jet", forms at the top of the bubble (see, for example, Plesset and Chapman (1971), Mitchell and Hammitt (1973), Lauterborn and Bolle (1975), and Blake et al. (1993)). Figure 1b shows the evolution of an initially spherical bubble collapsing near a wall in an initially quiescent fluid. The bubble is shown at nine equal time intervals and the figure clearly shows the re-entrant jet forming on the top of the bubble as time increases. The cavitation model assumed that the pressure inside the bubble was equal to the vapor pressure.

6 DNS Results with Variable pressure inside the bubble

A more realistic cavitation model is the one in which the pressure inside the bubble is not constant but varies with the bubble volume, according to Equation 4. The pressure inside the bubble is composed of the vapor pressure and the partial pressure of the gases. While the vapor pressure remains constant, the partial pressure of the gases decreases as the bubble volume increases and its effect on the bubble diminishes as the bubble grows. This cavitation model is more realistic because bubbles contain non-condensable gases too, and it is the presence of the non-condensable gases that maintains pressure equilibrium in the bubble before

it is captured by the vortex. DNS of a cavitating bubble with various Weber numbers and cavitation numbers were performed using this updated cavitation model. The pressure inside the bubble was initially set such that the bubble was in pressure equilibrium at the start of the computation. Figures 2a and 2b present the effect of the bubble and core diameter ratio on the growth of the bubble. In Figure 2a, the ratio D_{core}/D_b is 8 and in Figure 2b, the ratio In both figures the Weber number was 24, the cavitation number was 0.5, and results are shown at dimensionless time. As expected, the bubble with a higher initial diameter grows to a larger volume than the bubble with a smaller initial diameter. Figures 3a, 3b, and 3c show front, top, and side view images of a bubble with $D_{core}/D_b = 4$, $We = 24$, and $\sigma = 0.5$ at time $t/(L/2U_{core}) = 1.2$. It can be observed that the bubble does not keep its initial spherical shape but tends to elongate along the axis of the vortex, eventually filling the vortex. Figures 4a shows the effect of the Weber number on the growth, respect of a bubble with $D_{core}/D_b = 8$, $x/L = 0.2$, $D_{core}/L = 0.5$. For a cavitation number of 0.5, the bubble grows as it gets trapped by the vortex, and the bubble with the highest Weber number, which implies the smallest surface tension, grows more rapidly than the bubbles with smaller Weber numbers. Figures 4b and 4c show a comparison between the two bubble/core diameter ratios used, $D_{core}/D_b = 8$ and 4, for a bubble with Weber number of 24. For a cavitating number of 0.5, both bubbles grow and the growth rate of the bubble with $D_{core}/D_b = 4$ is much faster than the growth rate of the bubble with $D_{core}/D_b = 8$. Table (a) shows the bubble capture time for the bubbles that grow as they are trapped by the vortex. The bubbles have a core diameter to bubble diameter ratio $D_{core}/D_b = 8$ and an initial position of x/L=0.2. The capture time for cavitating bubble is defined based on the bubble volume. The bubbles with $D_{core}/D_b = 8$ have an initial volume of 0.0127% of the computational domain volume at time 0. These bubbles are considered to be captured by the vortex when their volume reaches 800 times the initial bubble volume. The bubbles with $D_{core}/D_b = 4$ have an initial volume of 0.102% of the computational domain volume at time 0. These bubbles are considered to be captured by the vortex when their volume reaches 70 times the initial bubble volume. These capture criteria were chosen because by the time the bubbles reach the specified volume their diameter is almost equal to the diameter of the vortex. Table (b) shows similar results for bubbles with a core diameter to bubble diameter ratio $D_{core}/D_b = 4$ and x/L=0.2.

Table a. Bubble capture time for $D_{core}/D_b = 8$, x/L=0.2.

We	σ	t/(L/2 U_{core})
23.4	0.1	1.0
23.4	0.17	1.1
23.4	0.5	1.3
93.6	0.5	1.26
12	0.5	1.33

Table b. Bubble capture time for $D_{core}/D_b = 4$, x/L=0.2.

We	σ	t/(L/2 U_{core})
187	0.5	0.97
187	0.1	1.43
24	0.5	1.02
24	1	1.53

7 Comparison between DNS and PT for Cavitating Bubbles

The DNS results for the trajectory and growth rate of the cavitating cavitating bubble as it gets trapped by the vortex were compared to the particle-tracking model, Equation 7, that includes the force term that deals with the bubble volume variation. The bubble volume was computed by integrating the Rayleigh-Plesset Equation 9. Figure 5a shows a comparison between the DNS results and the particle-tracking (PT) model for

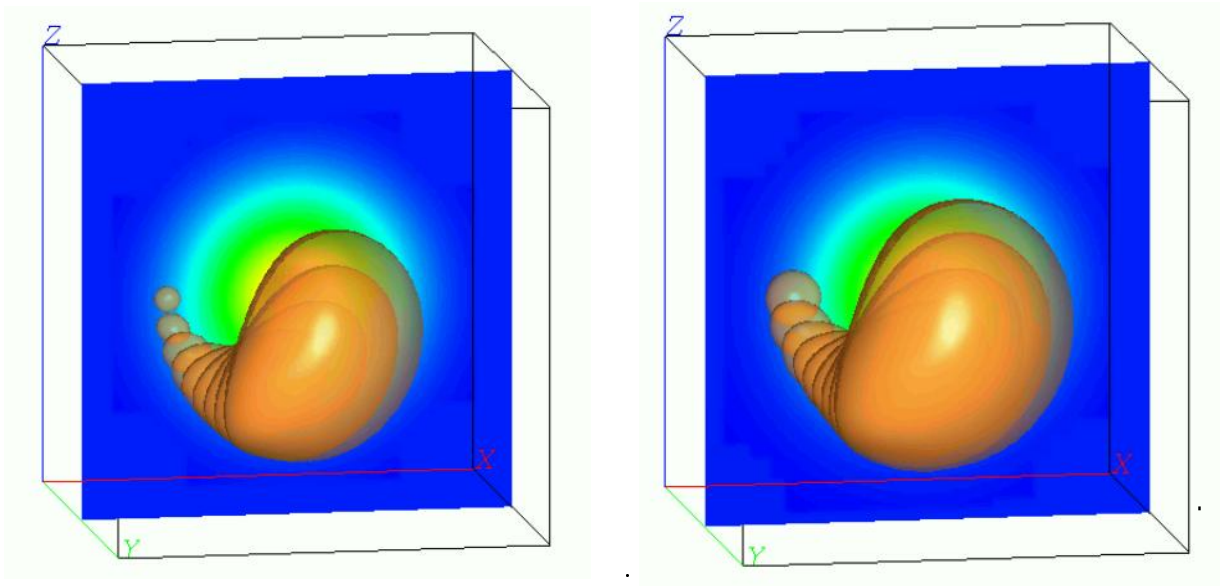

Figure 2: Bubble growth 2a Left: $D_{core}/D_b = 8$. 2b Right: $D_{core}/D_b = 4$. For both figures: x/L=0.2, $We = 24$, $\sigma = 0.5$, $D_{core}/L = 0.5$ $t/(L/2U_{core}) = 1.2$. Red corresponds to a dimensionless vorticity value of 8 and blue to a value of 0.

the case of a bubble with $D_{core}/D_b = 8$, $We = 23.4$, $D_{core}/L = 0.5$, $\sigma = 0.5$, $t = 1.07$. The PT model does not include a lift force in this computation. Figure 5b shows the bubble volume growth rate for the DNS and the PT model results. It can be observed that the PT model yields a higher bubble growth rate than the DNS. One drawback of the PT model is that the bubble is considered to be spherical and as shown above (see Figures 3a,3b, and 3c) the bubble does not remain spherical during the capture process but elongates along the vortex axis. The calculation of the ambient pressure, p in Equation 9, is important for the PT model. In Figure 6a it is shown how the bubble volume growth rate varies depending on how the pressure outside the bubble is computed. When computing the pressure, p, by averaging the pressure at the surface of the bubble we obtain a better agreement with DNS results compared to using the value of the pressure in the center of the bubble. The best agreement is obtained when using 4 or 8 points on the bubble surface for averaging. By using 14 points no improvement is achieved. Figure 6a provides a comparison between the DNS result and the PT model for different lift coefficients in the PT model. For this simulation $\sigma = 0.5$, $D_{core}/D_b = 8$, We = 23.4, x/L = 0.2, $D_{core}/L = 0.5$, and time=0.88. The drag coefficient by Haberman and Morton (1953) was used. It can be observed that neither trajectory computed with the PT model agrees well with the DNS result. Figure 7a shows the same trajectory at a later time. Figure 7b presents the bubble volume growth rate for the simulations shown in Figure 7a and it can be noticed that the PT model predicts a much slower bubble volume growth rate than the DNS result. This difference emphasizes the fact that the PT model assumes that the bubble remains spherical while in the DNS results it was shown that the bubble actually deforms as it interacts with the vortex and elongates along the axis of the vortex.

8 Conclusions

The DNS results show that the shape of the bubbles can be significantly distorted as they are captured by a vortex. This distortion can lead to the creation of lift forces that shorten the capture time of the bubbles. Consequently, it is difficult to know precisely what lift coefficients should be selected for the particle-tracking models. On the model scale, the diameter of a vortex core will be on the order of 1mm, and the tangential velocity will be on the order 10 m/s. This yields a Reynolds number on the order of 10^4 for flows water. This is similar to the computed Reynolds number examined above. The bubbles computed had core diameter on the order of 100 μm. The nuclei actually range from 1 to 100 μm. Thus, these results are applicable to for

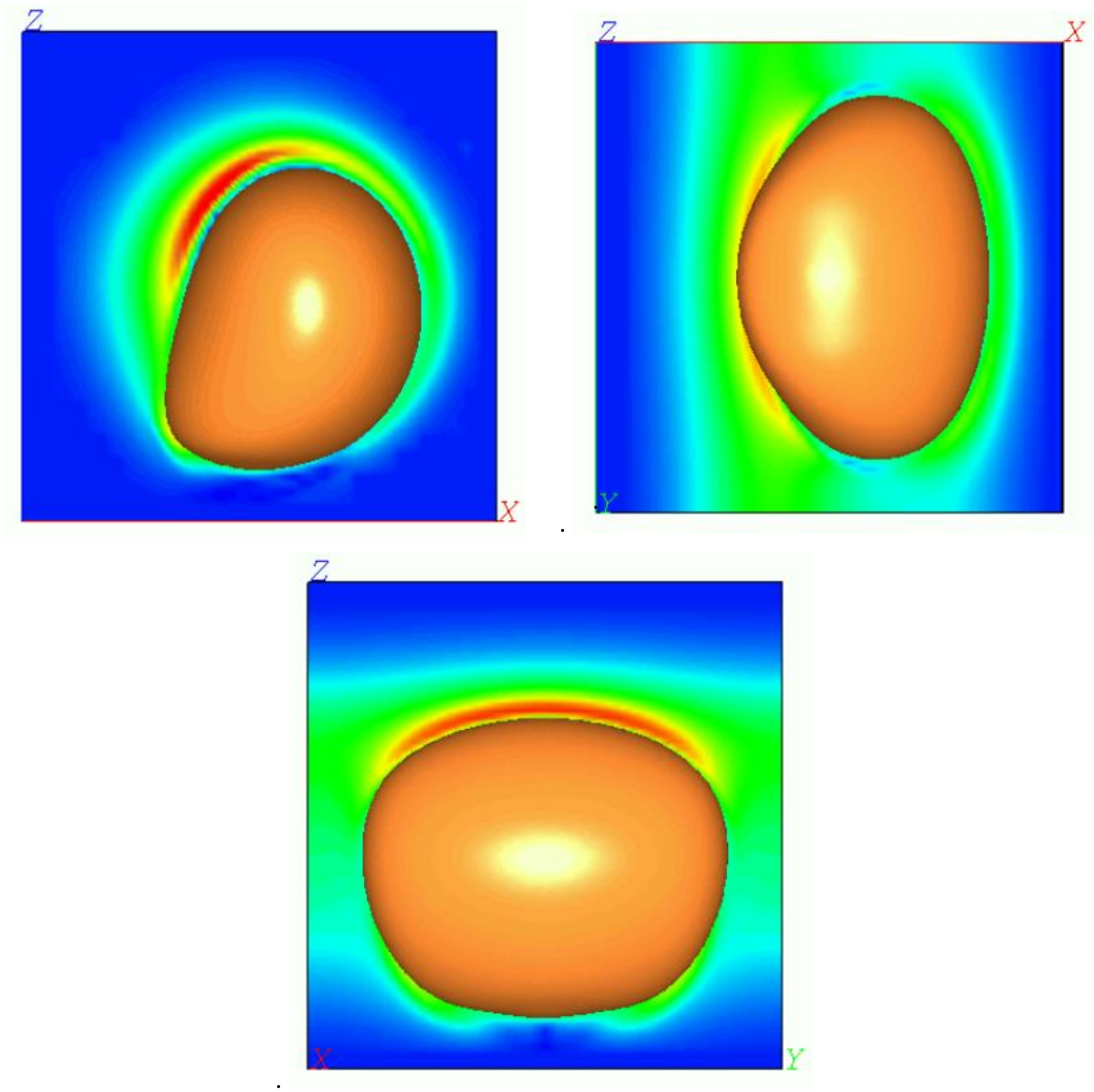

Figure 3: 3a Left: Front view of a bubble trapped in a vortex. 3b Center: Top view of a bubble trapped in a vortex. 3c Right: Side view of a bubble trapped in a vortex. For x/L=0.2, $W_e = 24$, $\sigma = 0.5$, $D_{core}/L = 0.5$ $t/(L/2U_{core}) = 1.2$. Red corresponds to a dimensionless vorticity value of 8 and blue to a value of 0.

the largest nuclei. A nucleus with diameter of 100 μm would represent a Weber number of about 350 for a clean bubble of air in water. This suggest that larger bubbles on the model scale may experience the larger deformations observed here. Conversely, a 1 μm diameter bubble would have a Weber number of about 3.5. The simulations were conducted for a vortex that is similar to a laboratory scale vortex with core size on the order of 1mm and tangential velocity on the order of 10 m/s. At full scale, the vortical flow may consist of a vortex with a 10 mm diameter core. Thus, the core/diameter ratio would become much larger (100 to 10000). It is therefore possible that the bubble capture mechanisms at full scale can be very different. The capture times varied over less than an order of magnitude for most cases, and this suggests that one might derive and average capture time of the PT models. The results of the PT model with different choices of the lift and drag coefficients, and more comparisons are needed to choose the best values of these parameters. The results of the particle tracking models can vary widely depending on the selected values of the lift and drag coefficients and nominal Weber number of the captured nucleus. For model scale flows, the Weber number may vary from 1 to 100. Thus, it is possible that a particle-tracking model should have variable lift

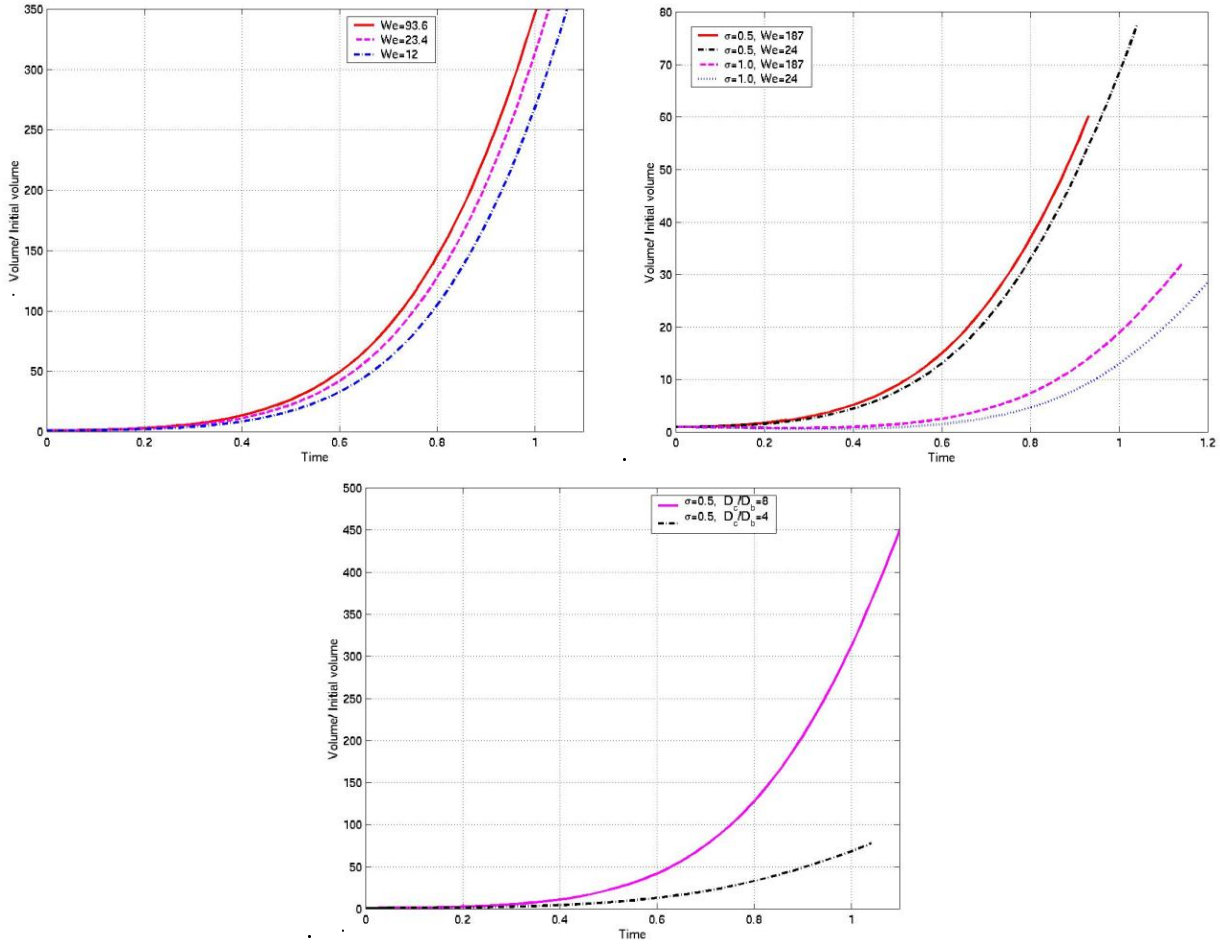

Figure 4: Growth of a Bubble in a Vortex ($D_{core}/L = 0.5$, x/L=0.2, : 4a Left: $D_{core}/D_b = 8$, $\sigma = 0.5$. 4b Center: $D_{core}/D_b = 4$. 4c Right: $D_{core}/D_b = 8$,$D_{core}/D_b = 8$,$\sigma = 0.5$

and drag coefficients that better take into account the estimated instantaneous bubble deformation. The drag coefficient by Haberman and Morton (1953) yielded a trajectory that was closer to the DNS trajectory than when using the drag coefficient given by Clift et al.(1978). It was determined that the lift coefficients given by Dandy and Dwyer (1990) and Auton et al. (1988) yielded capture times that were much bigger than the DNS results and that lift coefficient between the those given by Saffman (1965) and Dandy and Dwyer (1990) would give results that are closer to the DNS results.

Acknowledgements

This work was supported by the Office of Naval Research, contract N00014-99-1-0307, the Maui High Performance Computing Center, and GE Nuovo Pignone (Bari)

References

Blake, J.R., Taib, B.B., and Doherty, G.,(1986) *Transient Cavities near Boundaries. Part 1. Rigid Boundary*, J. Fluid Mech. Vol. 170, pp. 479-497.

Chahine, G.L., (1994), *Strong Interaction Bubble/Bubble and Bubble/Flow.* Bubble Dynamics and Interface Phenomena, J.R. Blake et al.(eds), pp 195-206

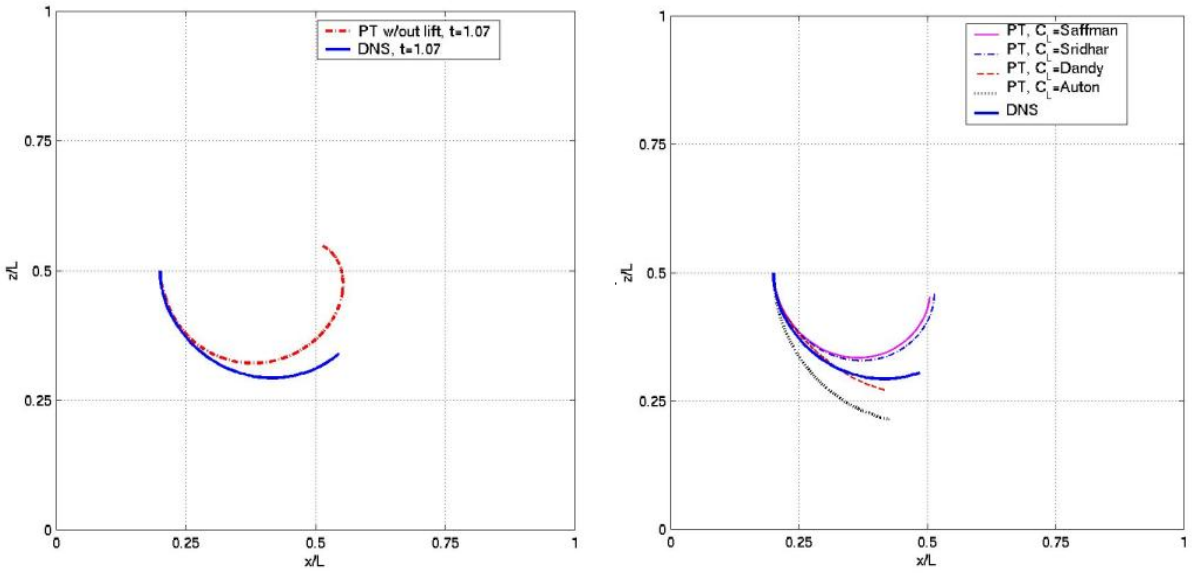

Figure 5: Comparison between DNS and PT for $D_{core}/D_b = 8$,x/L=0.2, $W_e = 24$, $\sigma = 0.5$, $D_{core}/L = 0.5$ 5a Left: Trajctoties calculated without Lift Coefficient. 5bRight: Trajctoties calculated with different Lift Coefficients

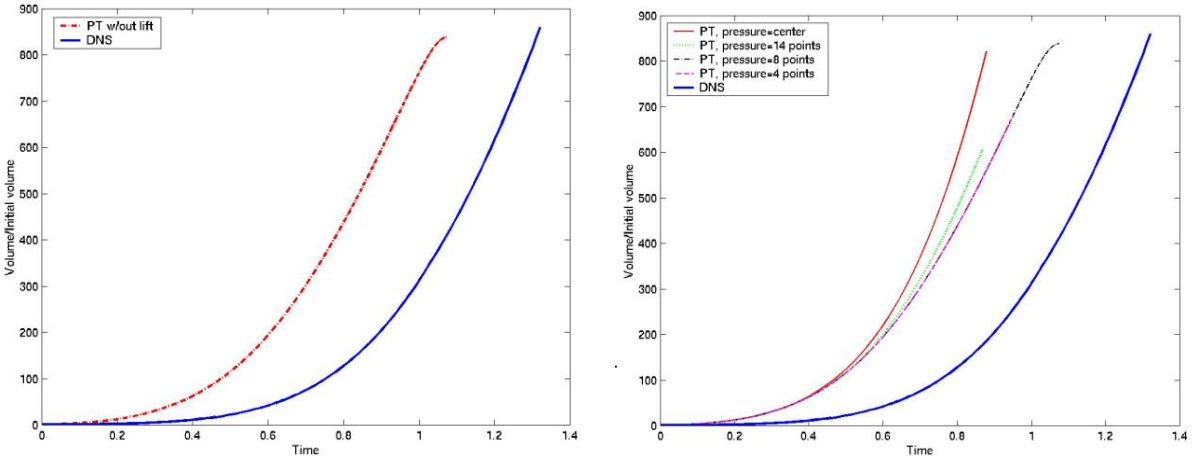

Figure 6: Comparison between DNS and PT for $D_{core}/D_b = 8$,x/L=0.2, $W_e = 24$, $\sigma = 0.5$, $D_{core}/L = 0.5$ 6a Left: Volume growth calculated without Lift Coefficient. 6b Right: Volume growth calculated averaging the pressure at the surface of the bubble different Lift Coefficients

Dandy, D.S. and Dwyer, H.A., (1990), *A Sphere in Shear Flow at Finite Reynolds Number: Effect of Shear on Particle Lift, Drag, and Heat Transfer*, J. of Fluid Mech., Vol. 216, pp. 381-410..

Esmaeeli, A., and Tryggvason, G., (1998), *Direct Numerical Simulations of Bubbly Flows. Part 1. Low Reynolds Number Arrays*, J. of Fluid Mech., Vol. 377, pp. 313-345.

Esmaeeli, A., and Tryggvason, G., (1999),*Direct Numerical Simulations of Bubbly Flows. Part 1. Moderate Reynolds Number Arrays*, J. of Fluid Mech., Vol. 385, pp. 325-358.

Haberman, W.L. and Morton, R.K., (1953), *An Experimental Investigation of the Drag and Shape of Air Bubbles Rising in Various Liquids*, DTMB Report 802.

Harlow, F.H. and Welch, J.E., (1965), *Numerical Calculation of Time-Dependent Viscous Incompressible Flow of Fluid with Free Surface*, Physics of Fluids, Vol. 8, pp. 2182-2189.

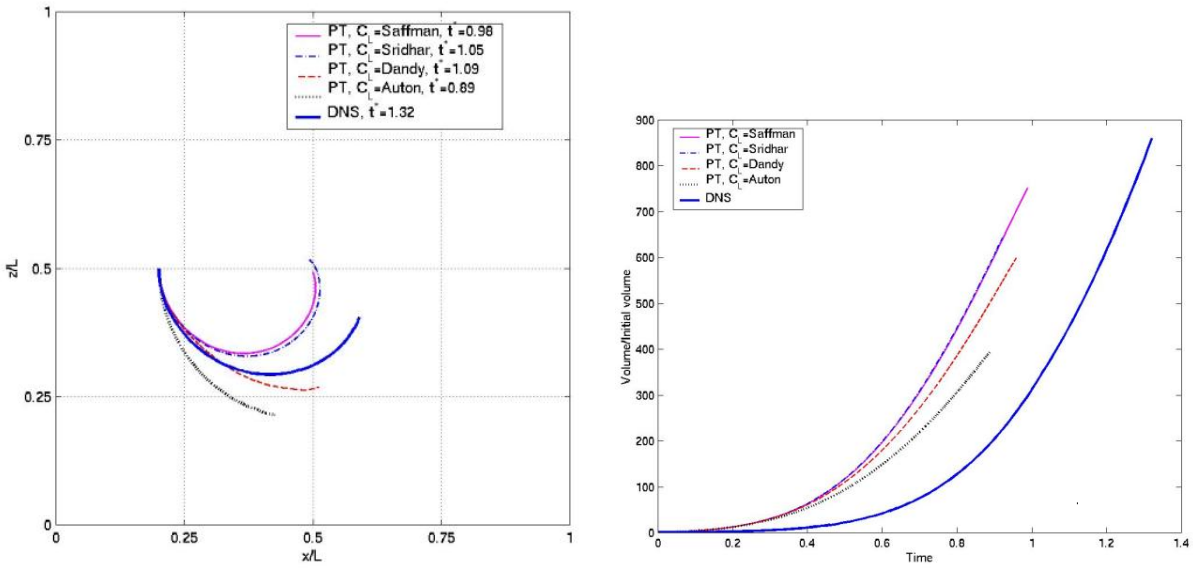

Figure 7: Comparison between DNS and PT for $D_{core}/D_b = 8$,x/L=0.2, $W_e = 24$, $\sigma = 0.5$, $D_{core}/L = 0.5$ 7a Left: Trajctoties. 7b Right: Volume growth

Hsiao C.T., Pauley L.L. (1999), *Study of Tip Vortex Cavitation Inception Using Navier-Stokes Computation and Bubble Dynamics Model*, Journal of Fluids Engineering 121(1): March 1999,198-204.

Johnson, V.E. and Hsieh, T., (1966), *he Influence of the Trajectories of Gas Nuclei on Cavitation Inception*, Proceedings of the Sixth Symposium on Naval Hydrodynamics, pp. 163-179.

Lamb, H., (1932), *Hydrodynamics*, 6th ed. Cambridge University Press.

Lauterborn, W. and Bolle, H., (1975), *Experimental Investigations of Cavitation-Bubble Collapse in the Neighborhood of a Solid Boundary*, J of Fluid Mech, Vol. 72, pp. 391-399.

Maxey, M.R. and Riley, J.J., (1983), *Equation of Motion for a Small Rigid Sphere in a Nonuniform Flow*, Physics of Fluids, Vol. 26, pp. 883-889.

Mitchell, T.M., and Hammitt, F.G., (1973), *Asymmetric Cavitation Bubble Collapse*, Trans. ASME I: J. of Fluids Engin., Vol. 95, pp. 29-37.

Naude, C.F. and Ellis, A.T., (1961), *On the Mechanism of Cavitation Damage by Nonhemispherical Cavities Collapsing in Contact with a Solid Boundary*, Journal of Basic Engineering, Trans. ASME D, Vol. 83, pp. 648-656.

Pannala, S. and Menon, S., (1997), *Numerical studies of Bubble Collapse and Rebound near a Wall*, Proceedings of the ASME Fluids Engineering Division Summer Meeting, FEDSM'97-3244.

Plesset, M.S., (1948), *Dynamics of Cavitation Bubbles*, Journal of Applied Mechanics, Vol. 16, pp. 228-231.

Rayleigh, L., (1917), *On the Pressure Developed in a Liquid During the Collapse of a Spherical Cavity*, Philosophical Magazine and Journal of Science, Vol. 34, pp. 94-98.

Saffman, P.G., (1992), *Vortex Dynamics*, Cambridge University Press.

Sridhar, G. and Katz, J., (1999), *Effect of Entrained Bubbles on the Structure of Vortex Rings* J. of Fluid Mech., Vol. 397, pp. 171-202.

Tong, R.P., (1998), *The Application of Boundary Integral Methods to Collapsing Bubbles* Proceedings of the ASME Fluids Engineering Division Summer Meeting, FEDSM98-5225.

Unverdi, S.O. and Tryggvason, G., (1992), *A Front-Tracking Method for Viscous, Incompressible, Multi-Fluid Flows* Journal of Computational Physics, Vol. 100, pp. 23-37.

Van der Meulen, J.H.J., (1994), *On Laser-Induced Cavitation Bubbles and the Impact on Nearby Solid Boundaries*, Proceedings of the 2nd International Symposium on Cavitation, April, Tokyo, Japan.